

## Two-Phase Flow Measurements in Un-stationary Free-surface Flows: a New Signal Decomposition Technique

Stefan Felder<sup>1</sup>, Hubert Chanson<sup>2</sup>

<sup>1</sup>The University of Queensland, School of Civil Engineering, Brisbane QLD4072, Australia

<sup>2</sup>The University of Queensland, School of Civil Engineering, Brisbane QLD4072, Australia

**Keywords:** air-water flow instabilities, triple decomposition, phase-detection probe, signal processing, turbulence characteristics, free-surface flows

### Abstract

In free-surface flows, some flow instabilities may be observed, for example in pooled stepped spillways and hydraulic jumps. These instabilities may include some pulsations and oscillations. Most traditional two-phase flow analyses would yield some air-water turbulent flow results combining the contributions of the slow fluctuations and of the turbulent motion. Herein a new turbulence decomposition technique was introduced to quantify the relative contributions of slow and fast fluctuations. The method was developed for and applied to phase-detection probe signals collected in highly-aerated free-surface flows. The interfacial velocity and turbulence properties were calculated based upon some advanced correlation analyses of the dual-tip probe signals. The triple decomposition results were applied to some un-stationary pooled stepped spillway flows and they highlighted that the gross turbulent kinetic energy was mostly encompassed in the slow fluctuating signal component. Altogether this study showed the successful application of a new decomposition technique suitable to gas-liquid flows in industrial applications with high void fractions.

### Introduction

Self-sustained instabilities and pseudo-periodic motion may be observed in free-surface aerated flows in hydraulic structures and industrial flows (Fig. 1). Documented examples include hydraulic jumps (Bradley and Peterka 1957), sloshing motion in a reservoir (Armenio and La Rocca 1996) and jump waves in pooled stepped spillways (Thorwarth 2008). On the Sorpe dam pooled stepped spillway (Germany), some pseudo-periodic flow were documented during some uncontrolled spillway release on 2 November 1998 (Chanson 2001). The self-sustained instabilities appeared at the spillway's upstream end and some jump waves propagated downstream, the surging waters overtopping the chute sidewalls and causing a hazard to nearby tourists (Fig. 1A). Thorwarth (2008) studied physically the unstable process described as jump waves. Mossa and Tolve (1998) and Leandro et al. (2012) studied the fluctuating of hydraulic jumps and the impact on the void fraction distribution and free-surface profile.

Herein a new triple decomposition technique is applied to phase-detection probe output signals, for the analyses of the velocity fluctuations in un-stationary free-surface flows. The application of the method can characterise both the fast turbulent and slow fluctuating velocity components. After a short description of the physical setup, some basic observations are shown in a stepped channel, before the triple decomposition technique is developed to some unstable air-water flows on a pooled stepped chute. The basic outcomes are presented later.



(A) Free-surface instability propagating down the Sorpe dam spillway (Germany) on 2 November 1998 (Courtesy of Ruhrverband) -  $\theta \approx 18^\circ$ ,  $h = 0.5$  to  $2$  m,  $Q = 6.9$  m<sup>3</sup>/s,  $Re = 1.0 \times 10^6$  - Note the children on the foreground right



(B) Free-surface instationarities in air-water flows on the pooled stepped spillway:  $\theta = 8.9^\circ$ ,  $h = 0.05$  m,  $q = 0.152$  m<sup>2</sup>/s,  $d_p/h = 2.66$ ,  $Re = 6.0 \times 10^5$

**Figure 1:** Free-surface instationarities in air-water free-surface flows

## Nomenclature

C	void fraction
c	instantaneous void fraction
$d_c$	critical flow depth (m): $d_c = (q^2/g)^{1/3}$
F	bubble count rate ( $s^{-1}$ )
g	gravitational constant ( $m s^{-2}$ )
h	vertical step height (m)
N	number of samples
n	number of interfaces
Q	water discharge ( $m^3 s^{-3}$ )
q	discharge per unit width ( $m s^{-2}$ )
Re	Reynolds number: $Re = \rho \times q / \mu$
$R_{xx}$	normalised auto-correlation coefficient
$R_{xy}$	normalised cross-correlation coefficient
T	average interface travel time between sensors (s)
$T_{xx}$	auto-correlation time scale (s)
$T_{xy}$	cross-correlation time scale (s)
Tu	turbulence intensity
V	interfacial velocity ( $m s^{-1}$ )
$V_c$	critical flow velocity ( $m s^{-1}$ ): $V_c = (q \times g)^{1/3}$
$v'$	turbulent velocity fluctuations ( $m s^{-1}$ )
y	normal distance (m) measured perpendicular to the pseudo-bottom formed by step edges

### Greek letters

$\Delta x$	longitudinal separation distance between sensors (m)
$\Delta z$	transverse separation distance between sensors (m)
$\mu$	water dynamic viscosity (Pas)
$\theta$	angle between chute slope and horizontal
$\rho$	water density ( $kg m^{-3}$ )
$\tau$	time lag (s)

### Subscripts

c	critical flow conditions
90	flow properties at $C = 0\%$

## Basic Signal Processing

In a free-surface flow, the void fraction ranges typically from 0 to 100%, as illustrated in Figure 1, and the mass and momentum fluxes are encompassed within the flow region with void fractions less than 95% (Cain 1978, Wood 1985). A number of physical data demonstrated that the high-velocity gas-liquid flows behave as a quasi-homogenous mixture and the two phases travel with a nearly identical velocity, the slip velocity being negligible (Rao and Kobus 1971, Cain and Wood 1981, Wood 1991, Chanson 1997). For such aerated flows, a robust metrology is the phase-detection needle probe (Fig. 2). The needle-shaped phase detection probe is designed to pierce the bubbles and droplets, and Figure 3 (Top) shows a typical signal output. In Figure 3 (Top), each steep drop of the signal corresponds to an air bubble pierced by the probe tip. Although the first needle probe designs were based upon resistivity probes, both optical fibre and resistivity probe systems are commonly used (Cartellier 1992, Chanson 2002).

In free-surface flows, the basic signal processing of the raw voltage signals is based upon a single threshold technique and some statistical analyses of the raw signal. The single threshold is typically between 40 and 50% of the air-water range (Toombes 2002, Chanson and Felder 2010) and the

basic outputs are the void fraction, bubble count rate and air/water chord sizes distributions.

A cross-correlation analysis between the two conductivity probe tip signals yields the time-averaged interfacial velocity  $V = \Delta x / T$ , where  $\Delta x$  is the distance between the probe sensors and  $T$  is the time lag for which the cross-correlation function is maximum ( $R_{xy}$ )<sub>max</sub> (Herringe and Davis 1976, Chanson, 1997). The shape of the cross-correlation function provided further information on the velocity fluctuations. The integration of the auto- and cross-correlation functions from the maximum correlation to the first zero-crossing yields the correlation integral time scales  $T_{xx}$  and  $T_{xy}$ :

$$T_{xx} = \int_{\tau=\tau(R_{xx}=0)}^{\tau=0} R_{xx}(\tau) \times d\tau \quad (1)$$

$$T_{xy} = \int_{\tau=\tau(R_{xy}=(R_{xy})_{max})}^{\tau=\tau(R_{xy}=0)} R_{xy}(\tau) \times d\tau \quad (2)$$

The turbulence intensity is defined as the ratio of the velocity standard deviation to the time-averaged velocity:  $Tu = v' / V$ . When the velocity is measured with a dual-tip probe, the standard deviation of the interfacial velocity equals:

$$v'^2 = \frac{1}{n} \times \sum_{i=1}^n (v_i - V)^2 = \frac{V^2}{n} \times \sum_{i=1}^n \left( \frac{t_i - T}{t_i} \right)^2 \quad (3)$$

where  $v_i$  is the instantaneous velocity data equal to  $\Delta x / t_i$ ,  $V$  is the time-averaged velocity ( $V = \Delta x / T$ ),  $n$  is the number of interfaces,  $t_i$  is the interface travel time data and  $T$  is the travel time for which the cross-correlation function is maximum. With an infinitely large number  $n$  of interfaces, an extension of the mean value theorem for definite integrals may be used as  $1/t_i^2$  and  $(t_i - T)^2$  are positive and continuous functions over the interval  $i = (1, n)$  (Spiegel 1974). The result implies that there exists at least one characteristic travel time  $t'$  satisfying  $t_1 < t' < t_n$  such that:

$$\left( \frac{v'}{V} \right)^2 = \frac{1}{n} \times \frac{1}{t'^2} \times \sum_{i=1}^n (t_i - T)^2 = \frac{\sigma_t^2}{t'^2} \quad (4)$$

where  $\sigma_t$  is the standard deviation of the interface travel time. If the intrinsic noise of the probe signal is un-correlated to the turbulent velocity fluctuations with which the bubbles are convected, the standard deviation of the cross-correlation function  $\sigma_{xy}$  satisfies:

$$\sigma_{xy}^2 = \sigma_{xx}^2 + \sigma_t^2 \quad (5)$$

where  $\sigma_{xx}$  is the standard deviation of the autocorrelation function (Harvey 1993). The turbulence intensity becomes:

$$\frac{v'}{V} = \frac{\sqrt{\sigma_{xy}^2 - \sigma_{xx}^2}}{t'} \quad (6)$$

Assuming that  $t' \sim T$ , the turbulence intensity  $v' / V$  equals:

$$Tu = \frac{v'}{V} = \frac{\sqrt{\sigma_{xy}^2 - \sigma_{xx}^2}}{T} \quad (7)$$

Kipphan (1977) developed a similar result for two-phase mixtures such as pneumatic conveying, while the above development follows Chanson and Toombes (2002).

Assuming that the successive detections of bubbles by the probe sensors is a true random process, the cross-correlation function is a Gaussian distribution:

$$R_{xy}(\tau) = (R_{xy})_{max} \times \exp \left( -\frac{1}{2} \times \left( \frac{\tau - T}{\sigma_{xy}} \right)^2 \right) \quad (8)$$

After simplification the cross-correlation time scale becomes:

$$T_{xy} = (R_{xy})_{\max} \times \sqrt{\frac{\pi}{2}} \times \sigma_{xy} \quad (9)$$

Similarly, if the auto-correlation function is a Gaussian distribution, the auto-correlation time scale becomes:

$$T_{xx} = \sqrt{\frac{\pi}{2}} \times \sigma_{xx} \quad (10)$$

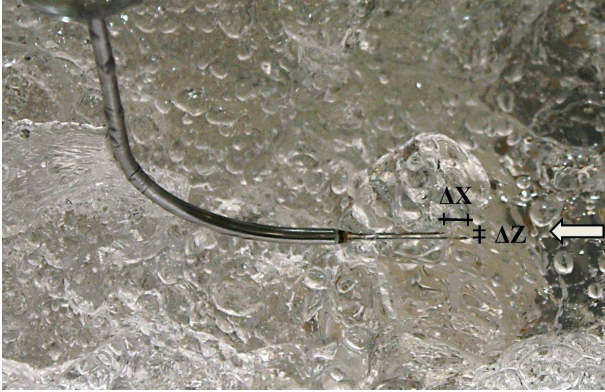


**Figure 2:** Two-tip phase-detection needle probe ( $\varnothing = 0.13$  mm) - Flow from right to left, with the definition of the probe sensor separation distances  $\Delta x$  and  $\Delta z$

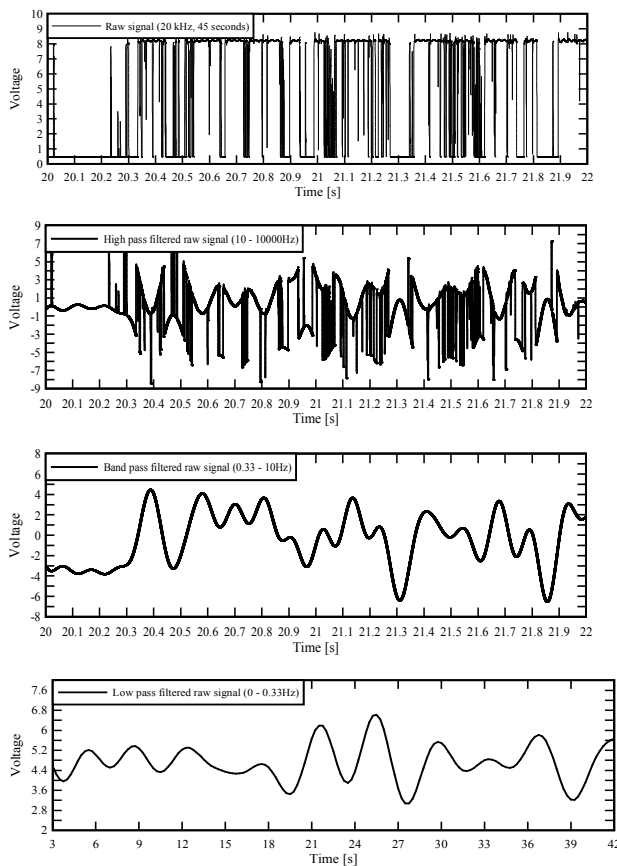


**Figure 3:** Raw and filtered signals on a pooled stepped spillway with flow instabilities:  $q = 0.182 \text{ m}^2/\text{s}$ , step 20,  $C = 0.445$ ,  $V = 2.55 \text{ m/s}$ ,  $F = 70.1 \text{ Hz}$  - Note the different scale for low pass filtered signal in the bottom graph

Using Equations (9) and (10), the turbulent intensity may be expressed as:

$$Tu = \frac{\sqrt{2}}{\sqrt{\pi} \times T} \times \sqrt{\left(\frac{T_{xy}}{(R_{xy})_{\max}}\right)^2 - T_{xx}^2} \quad (11)$$

Defining  $\tau_{0.5}$  the time scale for which:  $R_{xy}(T+\tau_{0.5})=R_{xy}(T)/2$ , the standard deviation of the cross-correlation function equals:  $\sigma_{xy} = \tau_{0.5}/1.175$ , while the standard deviation of the autocorrelation function equals:  $\sigma_{xx} = T_{0.5}/1.175$  where  $T_{0.5}$  is the characteristic time for which the normalised auto-correlation function equals 0.5. Equation (11) yields (Chanson and Toombes 2002):

$$\frac{v'}{V} = 0.851 \times \frac{\sqrt{\tau_{0.5}^2 - T_{0.5}^2}}{T} \quad (12)$$

### Signal Decomposition Technique

When a monophasic flow motion is characterised by slow fluctuations, the instantaneous velocity signal may be decomposed to quantify the respective contribution of the slow and fast fluctuations to the gross turbulent kinetic energy (Hussain and Reynolds 1972, Fox et al. 2005, Brown and Chanson 2013). With a phase-detection intrusive probe, the interfacial velocity signal is not continuous. Herein a triple decomposition method is developed and applied to the raw probe signals of a dual-tip conductivity probe (Fig. 3). The probe signal is split into three components reflecting the mean, slow fluctuating and fast fluctuating contributions. The approach is somewhat similar to the mono-phase flow triple decomposition technique, but applied to the phase-detection probe signal. The signal decomposition is performed using some characteristic cut-off frequencies which must be identified: e.g., using visual observations as well as power spectra analyses of raw signals.

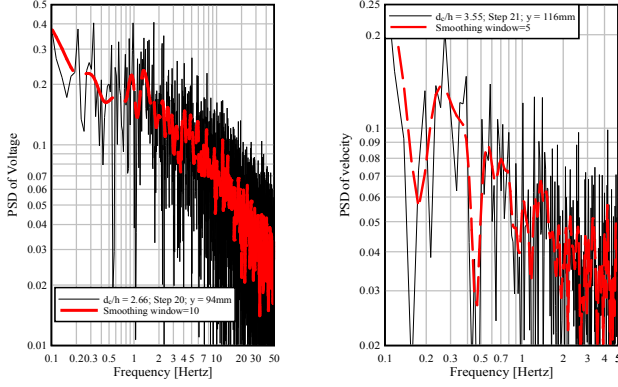
Note that some approach to the proposed decomposition is commonly performed in acoustics where it is called interaural correlation (Trahiotis et al. 2005, Boemer et al. 2011) and in speech recognition (Stern et al. 2007). In fluid mechanics, the correlation analysis of filtered signals is less common, although discussed by Favre (1965), Comte-Bellot and Corrsin (1971) and Frisch (1995).

### Characteristic Frequencies and Signal Decomposition

Some characteristic flow frequencies must be identified by visual observations of the air-water flow processes. In the present study, some physical experiments were conducted in a stepped pooled spillway chute (Fig. 1B & 4). Self-sustained instabilities were observed with typical frequencies within 0.5-2 Hz. These were seen in the FFT spectral analyses of the probe signals sampled (Fig. 5). Figure 5A shows a typical power spectrum density function of probe signal, highlighting some peaks and troughs in power spectrum density within 0.3-2 Hz. Some characteristic frequencies of about 0.3-0.5 Hz were also observed in the power spectrum of interfacial velocities, calculated by correlation analyses for short time periods of 0.1 s (10 Hz) (Fig. 5B). For the present data set, a sensitivity analysis was performed in terms of cut-off frequencies and the results yielded a meaningful lower cut-off frequency of 0.33 Hz and an upper cut-off frequency of 10 Hz. Thereafter the mean signal was the low pass filtered component with a cut-off frequency of 0.33 Hz, and the slow fluctuating signal was a band pass filtered component with upper and lower cut-off frequencies of 10 Hz and 0.33 Hz respectively.



**Figure 4:** Instationarities in skimming flows on the pooled stepped spillway:  $\theta = 8.9^\circ$ ,  $h = 0.05$  m,  $q = 0.122$  m<sup>2</sup>/s,  $d_c/h = 2.3$ ,  $Re = 4.9 \times 10^5$



(A) FFT of raw probe signal (B) FFT of interfacial velocity fluctuations (0.1 s intervals)

**Figure 5:** Spectral analysis of characteristic fluctuations of raw signals and interfacial velocities of a double-tip conductivity probe

The low pass, band pass and high pass filtering of the raw signals were calculated following Press et al. (2007). Figure 3 illustrates a typical raw probe signal and the resulting components after filtering (Fig. 3, Top to Bottom). The data set was based upon a complete time series of 39 s at 20 kHz, a 13 s sub-sample being used for proper smoothing.

#### Decomposition of the Air-Water Properties

The instantaneous void fraction may be expressed as a linear decomposition of filtered components:

$$c = \tilde{c} + c' + c'' \quad (13)$$

where  $c$  is the instantaneous void fraction,  $\tilde{c}$  is a mean or low pass filtered component,  $c'$  represents the slow fluctuating or band pass filtered contribution and  $c''$  is the fast fluctuating or high pass filtered component which is expected to be associated with the 'true' turbulent motion of the flow. The time averaged void fraction  $C$  is:

$$C = \frac{1}{N} \times \sum_1^N (\tilde{c} + c' + c'') = \tilde{C} + C' + C'' \quad (14)$$

where  $N$  is the number of samples. When the lower cut-off frequency (0.33 Hz herein) is significantly smaller than the characteristic frequencies of the air-water flow fluctuations, it yields:

$$C \approx \frac{1}{N} \times \sum_1^N \tilde{c} = \tilde{C} \quad (15)$$

$$C' = \frac{1}{N} \times \sum_1^N c' \approx 0 \quad (16)$$

$$C'' = \frac{1}{N} \times \sum_1^N c'' \approx 0 \quad (17)$$

The calculations of time-averaged velocity, turbulence intensity and auto- and cross-correlation time scales are based upon some auto- and cross-correlation analyses. Using normalised auto- and cross-correlation functions and assuming  $\tilde{c} \approx C$ , the decomposed auto- and cross-correlation functions may be linearly decomposed:

$$R_{xx}(\tau) = \alpha \times R_{x'x'}(\tau) + \beta \times R_{x''x''}(\tau) + \gamma \times (R_{x'x''}(\tau) + R_{x''x'}(\tau)) \quad (18)$$

$$R_{xy}(\tau) = A \times R_{x'y'}(\tau) + B \times R_{x''y''}(\tau) + D \times R_{x'y''}(\tau) + E \times R_{x''y'}(\tau) \quad (19)$$

where  $R_{xx}$  and  $R_{xy}$  are the auto- and cross-correlation functions for the raw signal and the decomposed signals respectively, and the factors  $\alpha$ ,  $\beta$ ,  $\gamma$ ,  $A$ ,  $B$ ,  $D$  and  $E$  are coefficients of proportionality. In Equations (14) and (15), the subscripts  $x'$  and  $y'$  indicate the band pass filtered signal components of the leading and trailing probe sensors, and the subscripts  $x''$  and  $y''$  the high pass filtered components of the sensors. The correlation functions between band pass filtered and high pass filtered signals are negligible since  $R_{x'x''} \approx R_{x''x'} \approx R_{x'y''} \approx R_{x''y'} \approx 0$  (Felder and Chanson 2012). The auto-correlation functions may be simplified to:

$$R_{xx}(\tau) \approx \alpha \times R_{x'x'}(\tau) + \beta \times R_{x''x''}(\tau) = R_{xx}'(\tau) + R_{xx}''(\tau) = R_{xx}^{(1)}(\tau) \quad (20)$$

where  $R_{xx}'$  and  $R_{xx}''$  are the auto-correlation functions of band pass and high pass filtered signals, and  $R_{xx}^{(1)}$  is their sum:  $R_{xx}^{(1)} = R_{xx}' + R_{xx}''$ . Similarly Equation (19) becomes:

$$R_{xy}(\tau) \approx A \times R_{x'y'}(\tau) + B \times R_{x''y''}(\tau) = R_{xy}'(\tau) + R_{xy}''(\tau) = R_{xy}^{(1)}(\tau) \quad (21)$$

where  $R_{xy}'$  and  $R_{xy}''$  are proportional to the cross-correlation functions of band pass and high pass filtered signals, and  $R_{xy}^{(1)}$  is the sum of the band and high pass filtered correlation functions:  $R_{xy}^{(1)} = R_{xy}' + R_{xy}''$  (Fig. 6)

Following Equation (21), the cross-correlation function can be decomposed linearly, and the time-averaged interfacial velocity corresponding to the band pass and high pass filtered signal is:

$$V' = \frac{\Delta x}{T'} \sim V \quad (22)$$

$$V'' = \frac{\Delta x}{T''} \approx V \quad (23)$$

where  $T'$  and  $T''$  are the time lags for which  $R_{xy}'$  and  $R_{xy}''$  were maximum respectively (Fig. 6). A further time-averaged interfacial velocity is:

$$V^{(1)} = \frac{\Delta x}{T^{(1)}} = V \quad (24)$$

where  $T^{(1)}$  is the time for which the sum of the band and high pass filtered correlation functions ( $R_{xy}^{(1)} = R_{xy}' + R_{xy}''$ ) is maximum: i.e.,  $R_{xy}^{(1)}(T^{(1)}) = (R_{xy}^{(1)})_{\max}$ .

The decomposition of the auto- and cross-correlation functions of the filtered signals is a linear process (Eq. (20) and (21)), and the definition of the auto- and cross-correlation integral time scale becomes:

$$T_{xx} \approx \alpha \times T_{x'x'} + \beta \times T_{x''x''} = T_{xx}' + T_{xx}'' \approx T_{xx}^{(1)} \quad (25)$$

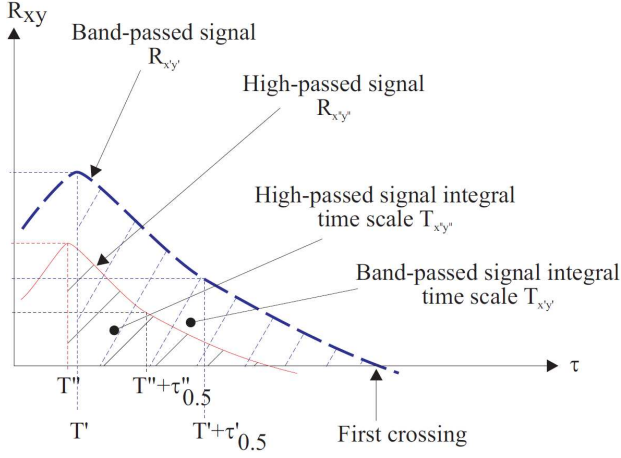
$$T_{xy} \approx A \times T_{x'y'} + B \times T_{x''y''} = T_{xy}' + T_{xy}'' \approx T_{xy}^{(1)} \quad (26)$$

where  $T_{xx}'$  and  $T_{xy}'$  are the auto- and cross-correlation time scales for the band pass filtered signal,  $T_{xx}''$  and  $T_{xy}''$  for the high pass filtered signal, and  $T_{xx}^{(1)}$  and  $T_{xy}^{(1)}$  for the sum of the band pass and high pass filtered correlation scales. The correlation time scales of the raw function were almost

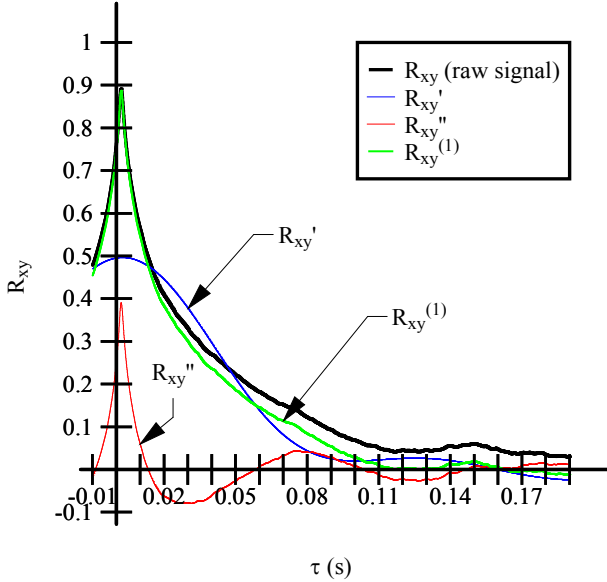
identical to the time scales  $T_{xx}^{(1)}$  (and  $T_{xy}^{(1)}$ ) and  $T_{xx}' + T_{xx}''$  (and  $T_{xy}' + T_{xy}''$ ) (Felder and Chanson 2012). That is:

$$T_{xx} \approx T_{xx}^{(1)} \approx T_{xx}' + T_{xx}'' \quad (27)$$

$$T_{xy} \approx T_{xy}^{(1)} \approx T_{xy}' + T_{xy}'' \quad (28)$$



(A) Definition sketch of cross-correlation functions of band-pass and high-pass filtered signals



(B) Cross-correlation functions of raw and filtered signals on the pooled stepped spillways - Flow conditions:  $\theta = 8.9^\circ$ ,  $h = 0.05$  m,  $q = 0.182$  m<sup>2</sup>/s,  $d_c/h = 3.0$ ,  $Re = 7.2 \times 10^5$ , step 20,  $y = 0.102$  m,  $C = 0.715$ ,  $F = 55.9$  Hz

**Figure 6:** Cross-correlation functions of phase-detection probe signal outputs

The turbulence intensity is deduced from the broadening of the cross-correlation function relative to the auto-correlation function. Herein the turbulence intensities for the band pass filtered, the high pass filtered signal and for the sum of the cross-correlation functions of band and high pass filtered signals are calculated as:

$$Tu' = 0.851 \times \frac{\sqrt{\tau'_{0.5}{}^2 - T'^{0.5}{}^2}}{T'} \quad (29)$$

$$Tu'' = 0.851 \times \frac{\sqrt{\tau''_{0.5}{}^2 - T''_{0.5}{}^2}}{T''} \quad (30)$$

$$Tu^{(1)} = 0.851 \times \frac{\sqrt{\tau_{0.5}^{(1)2} - T_{0.5}^{(1)2}}}{T^{(1)}} \quad (31)$$

While it is not possible yet to justify theoretically the validity of Equations (29) to (31) as the decomposition of Equation (12) is highly non-linear, the experimental results for all data sets (see below) show that the decomposition of the turbulence levels of the raw data is possible and the results yield:

$$Tu \approx Tu^{(1)} \quad (32)$$

### Comments

The auto- and cross-correlations of the probe signal components are valid representation of the original signal since a linear decomposition is applied (Eq. (20) & (21)). Yet it is not possible to prove the theoretical validity of the turbulence intensity decomposition because of the non-linearity of the calculation methods, although Equations (29) to (32) yield meaningful physical results. The present triple de-composition technique based upon the raw probe signals differs hence from the traditional triple decomposition of velocity signals.

### Basic Observations

New experiments were performed in a large size stepped spillway model previously used by Thorwarth (2008). The test section consisted of a 12 m long, 0.5 m wide channel equipped with 21 identical PVC steps, with height  $h = 0.05$  m and length  $l = 0.318$  m, corresponding to a channel slope  $\theta = 8.9^\circ$  (Fig. 1B & 4). Two step configurations were tested: flat steps and pooled steps with a pool weir height  $w = 0.05$  m (Fig. 4). Detailed two-phase flow measurements were conducted with a dual-tip conductivity probe ( $\varnothing = 0.13$  mm,  $\Delta x = 5.1$  mm,  $\Delta z = 1$  mm) (Fig. 2). The probe was mounted on a fine-adjustment traverse system enabling a vertical translation with an accuracy of 0.2 mm. The probe sensors were sampled at 20 kHz per sensor for 45 s. More details on the experimental facility and instrumentation can be found in Felder and Chanson (2012).

Visual observations were conducted for a range of discharges  $0.004 \leq q \leq 0.234$  m<sup>2</sup>/s ( $4 \times 10^3 < Re < 2.3 \times 10^5$ ). The air-water flow patterns on the flat stepped channel were comparable to previous studies on stepped spillways (Chanson 2001). For the smaller flow rates (i.e.  $d_c/h < 0.95$ ), a nappe flow regime was observed with a succession of free-falling jets, where  $d_c$  is the critical flow depth ( $d_c = (q^2/g)^{1/3}$ ). With increasing flow rate (i.e.  $0.95 < d_c/h < 1.69$ ), the flow appeared chaotic with some strong splashing in the transition flow regime. For larger flow rates  $d_c/h > 1.69$ , a skimming flow regime took place with stable cavity recirculation movements. The free-surface was parallel to the pseudo-bottom formed by the step edges in both aerated and non-aerated flow regions.

On the pooled stepped spillway, similar flow regimes were observed. That is, a nappe flow regime ( $d_c/h < 1.08$ ), a transition flow regime ( $1.08 \leq d_c/h \leq 1.76$ ) and a skimming flow regime ( $d_c/h > 1.76$ ) with increasing discharges. Some self-sustained instabilities were observed for  $d_c/h > 1.08$  up to the maximum flow rate in the present study ( $d_c/h = 3.55$ ). Self-induced jump waves were observed for  $1.08 \leq d_c/h \leq 1.76$ , at a frequency of about 0.25-0.4 Hz. The observation was close to the finding of Thorwarth (2008). Every second

jump wave was caused by some pulsating flows in the first step cavity. For larger discharges  $d_c/h > 1.76$ , the jump wave pattern was not clearly seen, but some instabilities were observed including unstable cavity recirculation, sudden cavity ejections and surface waves (Fig. 1B & 4). The instabilities appeared to decrease with increasing discharges. Through visual observations and video documentation, the unstable processes had characteristic frequencies in the range of 0.5 to 2 Hz.

### Air-water Flow Properties

Detailed air-water flow measurements were conducted for both stepped configurations for  $0.036 \leq q \leq 0.234 \text{ m}^2/\text{s}$  ( $3.6 \times 10^4 < \text{Re} < 2.3 \times 10^5$ ). On the flat stepped spillway, the pseudo-bottom ( $y = 0$ ) was defined by the step edges with  $y$  measured perpendicular to the pseudo-bottom. For the pooled stepped spillway, the datum ( $y = 0$ ) was the upper edge of the pool weir. A comparison between flat and pooled stepped spillway flows was performed for a wide range of discharges (Fig. 7 to 10). The void fraction distributions highlighted the strong aeration of the flow (Fig. 7). The profiles showed some typical S-shapes for both flat and pooled stepped spillways in skimming flows. Almost no difference was visible between the two stepped configurations (Fig. 7). Figure 7 shows a self-similar presentation with the void fraction  $C$  as a function of the dimensionless distance above the pseudo-bottom  $y/Y_{90}$  with  $Y_{90}$  the characteristic depth where the air concentration is 90%. The void fraction distributions compared very well with an analytical solution of the advective diffusion equation for air bubbles in turbulent free-surface flows (Chanson and Toombes 2002):

$$C = 1 - \tanh^2 \left( K' \frac{y/Y_{90}}{2 \times D_0} \right) + \frac{(y/Y_{90} - 1/3)^3}{3 \times D_0} \quad (33)$$

where  $K'$  is an integration constant and  $D_0$  is a function of the depth-averaged void fraction only. The interfacial velocity data for both stepped configurations exhibited some self-similar profiles in terms of  $V/V_{90}$  as a function of  $y/Y_{90}$ , where  $V_{90}$  is the velocity at  $C = 90\%$  (Fig. 7). Despite some data scatter, the velocity data were correlated with a power law:

$$\frac{V}{V_{90}} = \left( \frac{y}{Y_{90}} \right)^{1/m} \quad y/Y_{90} \leq 1 \quad (34)$$

The power law exponent was typically  $m = 10$ , but the exact value may vary from one step edge to the next one for a given flow rate. In the upper spray region (i.e.  $y/Y_{90} > 1$ ), a uniform velocity profile was observed:  $V/V_{90} = 1$ . Both functions are compared with experimental data in Figure 7. The distributions of bubble count rate showed characteristic shapes on both pooled and flat stepped spillways, with maximum values in the intermediate flow region ( $0.3 < C < 0.7$ ). In the bubbly flow region ( $C < 0.3$ ) and the spray region ( $C > 0.7$ ), the bubble frequency tended towards small values for large void/liquid fractions. The comparative analyses showed some marked differences between flat and pooled stepped spillways (Fig. 8). Figure 8 shows some typical dimensionless bubble count rate distributions  $F \times d_c/V_c$  for both configurations as a function of  $y/Y_{90}$  where  $F$  is the bubble count rate and  $V_c$  is the critical flow velocity. The dimensionless bubble frequencies of the flat stepped spillway were about twice as large as those recorded in the

pooled stepped spillway, across the entire air-water column. Some distinctive differences between pooled and flat spillway configurations were also observed in terms of the turbulence levels (Fig. 9). Figure 9 illustrates these differences in a self-similar presentation as a function of  $y/Y_{90}$ . On the pooled stepped spillway, the turbulence levels were drastically larger than on the flat stepped chute, and it is believed that this was linked with the presence of slow hydrodynamic fluctuations or hydrodynamic instabilities. The maximum turbulence levels reached up to 600% in the intermediate flow region on the pooled stepped spillway, compared to 150-200% on the flat stepped spillway. In the lower bubbly flow region and the upper spray region, the turbulence levels tended towards about 20-40% for both configurations as shown by Chanson and Toombes (2002).

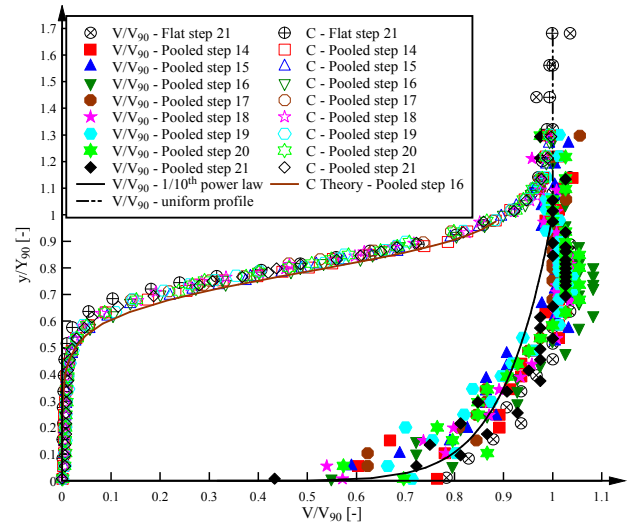


**Figure 7:** Dimensionless distributions of interfacial velocity and void fraction:  $q = 0.210 \text{ m}^2/\text{s}$ ,  $d_c/h = 3.3$ ,  $\text{Re} = 8.3 \times 10^5$

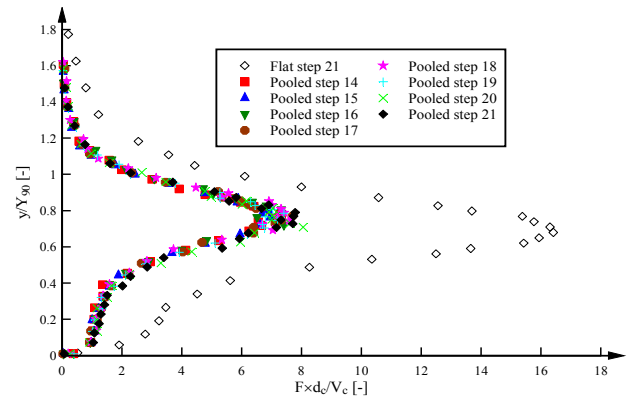


**Figure 8:** Dimensionless distributions of bubble count rate:  $q = 0.122 \text{ m}^2/\text{s}$ ,  $d_c/h = 2.3$ ,  $\text{Re} = 4.9 \times 10^5$

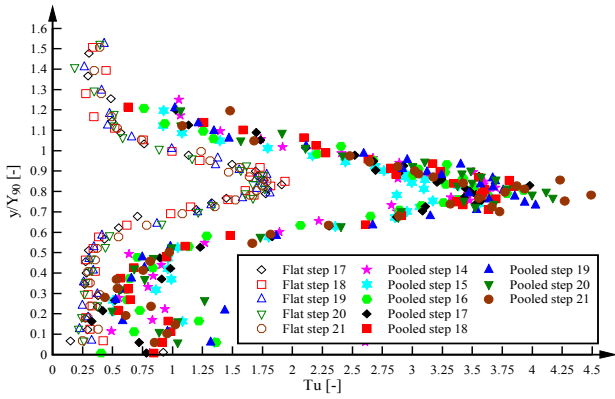
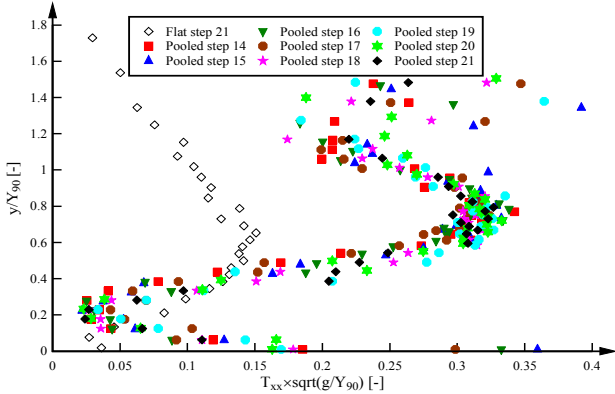
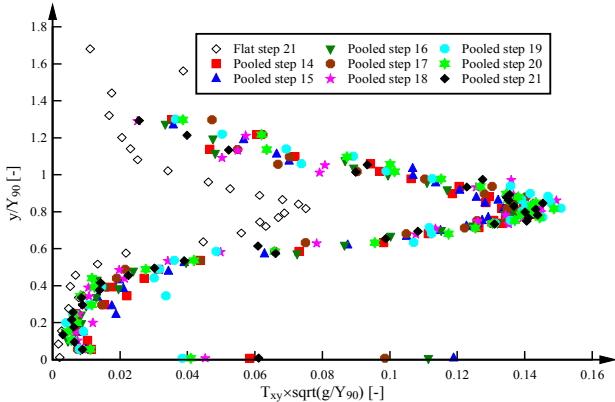


**Figure 9:** Distributions of turbulence intensity:  $q = 0.234 \text{ m}^2/\text{s}$ ,  $d_c/h = 3.55$ ,  $Re = 9.3 \times 10^5$



(A) Auto-correlation time scales:  $d_c/h = 1.35$ ,  $q = 0.055 \text{ m}^2/\text{s}$ ,  $Re = 2.2 \times 10^5$



(B) Cross-correlation time scales:  $d_c/h = 3.3$ ,  $q = 0.21 \text{ m}^2/\text{s}$ ,  $Re = 8.3 \times 10^5$

**Figure 10:** Dimensionless distributions of auto- and cross-correlation time scales

The auto- and cross-correlation integral time scale data showed also some differences between flat and pooled stepped chute flows (Fig. 10). In Figure 10A, the dimensionless auto-correlation time scales  $T_{xx} \times \sqrt{g/Y_{90}}$  are presented as a function of  $y/Y_{90}$ . The dimensionless time scales on the pooled stepped spillway were about three to four times larger than the time scales on the flat stepped spillway. A similar finding was seen in terms of the cross-correlation time scales  $T_{xy} \times \sqrt{g/Y_{90}}$  (Fig. 10B). The dimensionless cross-correlation integral time-scales were about five to seven times larger on the pooled stepped spillway.

### Application of the triple decomposition technique

The triple decomposition technique was applied to the raw probe signal data collected on the pooled stepped spillway. The cut-off frequencies were 0.33 and 10 Hz. The results below include the raw signal, the band pass filtered signal (or slow fluctuating signal), the high pass filtered signal (or fast fluctuating signal) and the calculations based upon the sum of slow and fast fluctuating signal correlations. In the following graphs, the notation reflects the decomposition method: e.g.,  $V$  the time-averaged interfacial velocity calculated from the raw signal,  $V'$  the slow fluctuating component of the velocity calculated from the band-pass filtered signal,  $V''$  the fast fluctuating velocity component computed from the high-pass filtered signal, and  $V^{(1)}$  the velocity calculated from the sum of correlation functions of band and high pass filtered signal components (Eq. (20) & (21)).

Figure 6B shows a typical cross-correlation function at one location in a skimming flow including the cross-correlation functions of the raw data  $R_{xy}$ , of the band pass filtered signal  $R_{xy}'$ , of the high pass filtered signal  $R_{xy}''$  and of the summation of the correlation functions of band and high pass filtered signals  $R_{xy}^{(1)}$ . The shapes of cross-correlation function were in agreement with previous results, although the time lag for first zero crossing was relatively longer. The sum of cross-correlation functions of band and high pass filtered components was close to the cross-correlation function of the raw signal, although the curve was slightly lower and crossed the x-axis for a smaller time lag.

The auto-correlation integral time scale data showed some difference in order of magnitude between the high pass filtered signal data  $T_{xx}''$  and the other components (Fig. 11). The auto-correlation time scale of the high pass filtered component was about one order of magnitude smaller than those of the other components, and the data trend suggested an increase in  $T_{xx}''$  with increasing void fraction. The auto-correlation time scales of the raw signal, the band pass filtered signal component and of the sum  $T_{xx}' + T_{xx}''$  were close, with maximum time scales in the intermediate flow region and smaller values in the lower bubbly and upper spray regions.

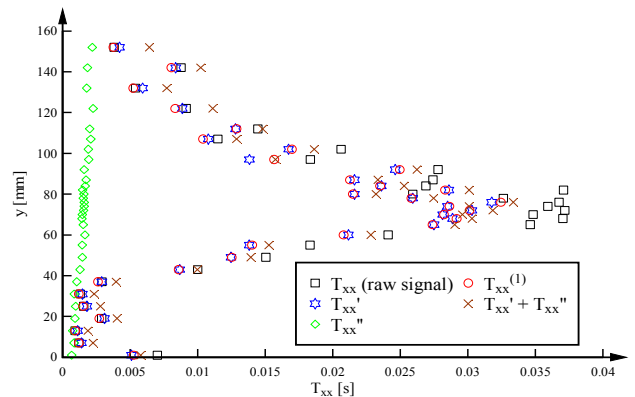


**Figure 11:** Distributions of auto-correlation time scales for the raw signal and the decomposed signal components:  $d_c/h = 2.3$ ,  $q = 0.122 \text{ m}^2/\text{s}$ ,  $Re = 4.9 \times 10^5$ ; step 18

Some typical cross-correlation integral time scale data are shown in Figure 12. The distribution shapes for the raw signal, the band pass filtered signal and the sum of the correlation functions of high and band pass filtered components were in good agreement, similar to previous

studies (Chanson and Carosi 2007, Felder and Chanson 2009). The largest integral time scale values were seen in the intermediate flow region, with  $T_{xy}$  tending towards zero in the bubbly flow region and smaller values of  $T_{xy}$  in the spray region. A different cross-correlation time scale shape was observed for the high pass filtered signal component.  $T_{xy}''$  tended to increase linearly with increasing distance from the pooled step edge. A further difference was the different order of magnitude for the high pass filtered data. In Figure 12, the data tended to highlight the linearity of the decomposition process for the cross-correlation time scales.

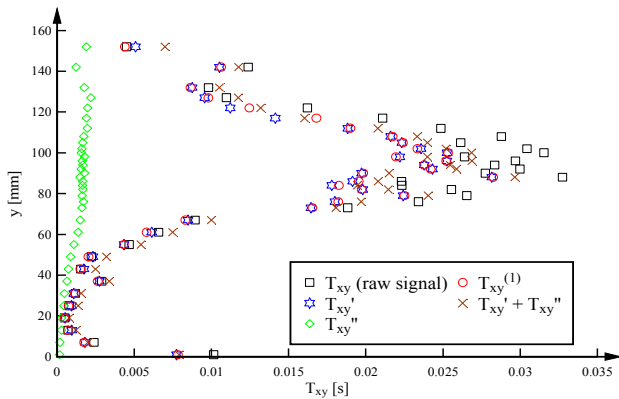


**Figure 12:** Distributions of cross-correlation time scales for the raw signal and the decomposed signal components:  $d_c/h = 3.0$ ,  $q = 0.182 \text{ m}^2/\text{s}$ ,  $Re = 7.2 \times 10^5$ ; step 20

Some typical results in terms of the time-averaged interfacial velocity are illustrated in Figure 13. The results for the raw signal, the fast fluctuating component and the sum of the correlation of band pass and high pass filtered signal components were basically identical. Further the velocity profiles were similar to previous studies on pooled stepped spillways (Kökpinar 2004, Thorwarth 2008). The distributions of the slow fluctuating velocity component  $V'$  exhibited some scatter in the bubbly and spray regions (Fig. 13). In the intermediate flow region, the velocity data were smaller compared to the raw signal analysis by about 10-15%. The differences might be linked with the cut-off frequency selection. The lower cut-off frequency of 0.33 Hz yielded a time scale (3 s) which was 2 to 3 orders of magnitude larger than the average interfacial travel time  $T$  between the probe sensors, while the upper cut-off frequency of 10 Hz (time scale: 0.1 s) corresponding to an average interfacial velocity of 0.5 m/s smaller than the typical interfacial velocity (2-3 m/s in Fig. 13). As such, the estimate of  $V'$  might have been adversely affected by the cutoff frequency selection.

Typical results of the signal's triple decomposition technique are presented in Figure 14 in terms of the turbulence intensity. The fast fluctuating turbulence intensity data  $Tu''$  had a shape close to that of the raw signal data  $Tu$ , with maxima in terms of turbulence intensity in the intermediate flow region (Fig. 14). However the fast fluctuating turbulence levels  $Tu''$  were smaller, with maximum values of about 120%, compared to 600% for the raw signal data. Some scatter of slow fluctuating turbulence data was observed, with values as large as 50% to 600%, and a majority of the data being within the range of 150% to 300%. The turbulence intensities calculated based upon the weighted sum of the correlation functions of band pass and

high pass filtered signal components were almost identical to the raw signal results:  $Tu \approx Tu^{(1)}$  (Eq. (32)). Furthermore the sum ( $Tu' + Tu''$ ) were close to the raw signal data for most positions as illustrated in Figure 14. Simply the present data suggested consistently that:

$$Tu \approx Tu^{(1)} \approx Tu' + Tu'' \quad (35)$$

Although no theoretical validation of Equation (35) was obtained, the experimental results showed that the triple decomposition technique yielded an accurate identification of the respective turbulence contributions of the slow and fast fluctuating velocity components. On the pooled stepped spillway, the physical data suggested that a large proportion of the turbulent kinetic energy was encompassed in the slow velocity motion and that  $Tu'' \ll Tu'$ . On average the present data yielded  $Tu''/Tu' = 0.56$  on the pooled stepped spillway.

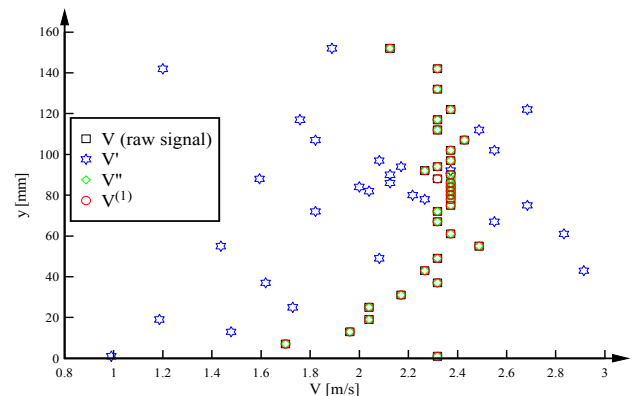


**Figure 13:** Distributions of interfacial velocities for the raw signal and the decomposed signal components:  $d_c/h = 2.66$ ,  $q = 0.152 \text{ m}^2/\text{s}$ ,  $Re = 6.0 \times 10^5$ ; step 19

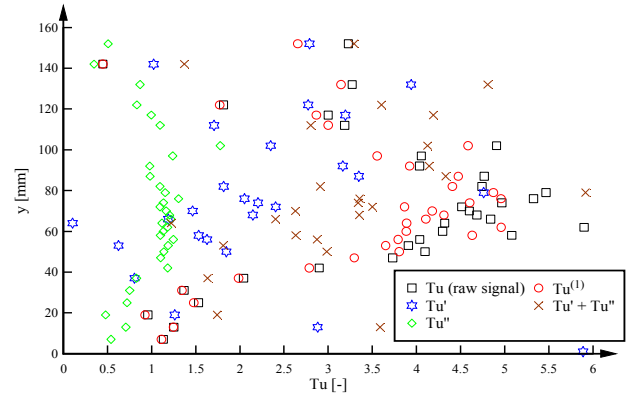


**Figure 14:** Distributions of turbulence intensities for the raw signal and the decomposed signal components:  $d_c/h = 1.7$ ,  $q = 0.078 \text{ m}^2/\text{s}$ ,  $Re = 3.1 \times 10^5$ ; step 17

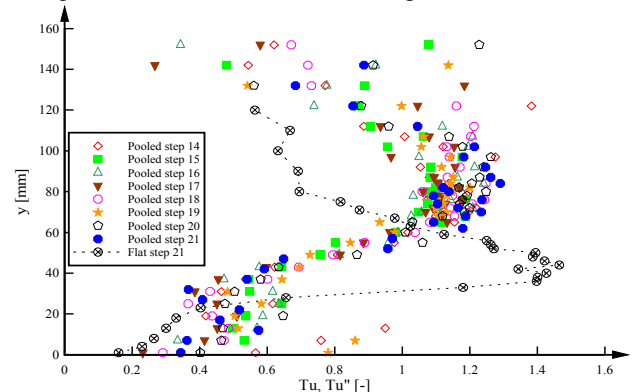


**Figure 15:** Comparison of turbulence intensity distributions of the fast fluctuating component ( $Tu''$ ) of the pooled

stepped spillway and of the flat stepped spillway (Tu):  $d_c/h = 2.3$ ,  $q = 0.122 \text{ m}^2/\text{s}$ ,  $Re = 4.9 \times 10^5$

## Discussion

The triple decomposition technique enabled the identification of the contributions of the various flow components into the turbulent kinetic energy. For the pooled stepped spillway, the slow fluctuating velocity component encompassed the largest contribution to the turbulent kinetic energy, while the velocity fluctuations in terms of fast fluctuating velocity component identified the "true" turbulence properties. For the pooled stepped spillway, the turbulence levels Tu" in terms of fast fluctuating velocity component may be compared with the turbulence intensity measurements Tu in flat stepped spillways with a same slope and for the same flow conditions (Fig. 15). Figure 15 shows a comparison in terms of turbulence levels on the flat stepped spillway and the fast fluctuating component on the pooled stepped spillway. All data sets were obtained for the same discharge and step height, and with the same instrumentation. The comparison suggested some qualitative agreement between the turbulence level distributions, while some quantitative differences in terms of vertical elevations were linked with differences in flow depths and the different definition of the pseudo-bottom: i.e., step edge for flat steps and pool edge for pooled steps.

## Conclusion

A decomposition technique was introduced herein to quantify the relative contributions of the slow- and fast fluctuations to the overall flow turbulence in a highly-aerated free-surface flow. The raw signal of the phase-detection probe leading and trailing tips was decomposed linearly into three components: a mean signal, a slow-fluctuating contribution and a fast-fluctuating component. The decomposition was based upon some signal filtering using characteristic cut-off frequencies. Some theoretical considerations suggested that the low pass filtered signal component did not contribute to the air-water flow properties, but the void fraction.

The results were applied to the analysis of physical experiments on a relatively large pooled stepped channel. The flow exhibited some self-sustained instabilities, with a range of characteristic frequencies between 0.5 to 2 Hz. Herein the cut-off frequencies of 0.33 Hz and 10 Hz were used. The triple decomposition results highlighted that the gross turbulent kinetic energy was mostly encompassed in the slow fluctuating signal component. The turbulence properties in terms of fast fluctuating signal component were qualitatively and quantitatively consistent with earlier findings of steady stationary air-water flows. Since the band pass filtering of the probe signal was a linear process, it was shown that little information was lost during the decomposition. The auto- and cross-correlation functions of each probe signal component were valid representation of the original signal, and the calculation of the time averaged interfacial velocities and the turbulence levels of the fast and slow fluctuating signal components may be performed.

Altogether this study showed the successful application of a new decomposition technique suitable to gas-liquid flows in industrial applications with high void fractions. To date the

method was applied to pooled stepped spillway, and it is believed that there are further potential applications to pseudo-periodic and unstable gas-liquid flows.

## Acknowledgements

The authors thank Prof. Jorge Matos (IST Lisbon) and Dr. Frédéric Murzyn (ESTACA Laval) for their valuable comments, and Prof. Schüttrumpf (RWTH Aachen University) for providing access to the experimental facility. The first author acknowledges the support through a UQ research scholarship and the (UQ) Graduate School International Travel Award. The financial support of the Australian Research Council (Grant DP120100481) is acknowledged.

## References

- Armenio, A., La Rocca, M. 1996. On the analysis of sloshing of water in rectangular containers: Numerical study and experimental validation. *Ocean Eng.*, Vol. 23, No. 8, pp. 705-739 (DOI: 10.1016/0029-8018(96)84409-X).
- Boemer, J.I., Oode, S., Ando, A., 2011. Effect of frequency bandwidth on interaural cross-correlation in relation to sound image width of reproduced sounds of a violin. *Applied Acoustics*, 72, 623–631.
- Bradley, J.N., Peterka, A.J. 1957. The Hydraulic Design of Stilling Basins: Stilling basin and wave Suppressors for Canal Structures, Outlet Works and Diversion Dams (Basin IV). *Jl of Hyd. Div., ASCE*, Vol. 83, No. HY5, pp. 1404-1/1404-20.
- Brown, R., Chanson, H., 2013. Turbulence and Suspended Sediment Measurements in an Urban Environment during the Brisbane River Flood of January 2011. *J. Hydraul. Eng., ASCE*, Vol. 139, No. 2, posted online ahead of print August 7, 2012 (doi: 10.1061/(ASCE)HY.1943-7900.0000666).
- Cain, P. 1978. Measurements within Self-Aerated Flow on a Large Spillway. Ph.D. Thesis, Ref. 78-18, Dept. of Civil Engrg., Univ. of Canterbury, Christchurch, New Zealand.
- Cain, P., Wood, I.R. 1981. Measurements of Self-aerated Flow on a Spillway. *Jl. Hyd. Div., ASCE*, 107, HY11, pp. 1425-1444.
- Cartellier, A. 1992. Simultaneous Void Fraction Measurement, Bubble Velocity, and Size Estimate using a Single Optical Probe in Gas-Liquid Two-Phase Flows. *Rev. Sci. Instrum.*, Vol. 63, No. 11, pp. 5442-5453.
- Chanson, H., 1997. *Air Bubble Entrainment in Free-Surface Turbulent Shear Flows*. Academic Press, London, UK, 401 pages.
- Chanson, H., 2001. *The Hydraulics of Stepped Chutes and Spillways*. Balkema, Lisse, The Netherlands, 418 pages.
- Chanson, H. 2002. Air-Water Flow Measurements with Intrusive Phase-Detection Probes. Can we Improve their Interpretation? *Journal of Hydraulic Engineering, ASCE*,

Vol. 128, No. 3, pp. 252-255

Chanson, H., Carosi, G., 2007. Turbulent time and length scale measurements in high-velocity open channel flows. *Exp. Fluids*, 42, 385-401 (DOI 10.1007/s00348-006-0246-2).

Chanson, H., Felder, S., 2010. Turbulence Measurements in Air-Water Self-Aerated Flows: Basic Analysis and Results. Proc. 7th International Conference on Multiphase Flow ICMF 2010, Tampa FL, USA, May 30-June 4, Paper No. 10.3.4, 11 pages (USB Memory Stick).

Chanson, H., Toombes, L., 2002. Air-Water Flows down Stepped chutes: Turbulence and Flow Structure Observations. *Intl. J. Multiphase Flow*, 28, 1737-1761.

Comte-Bellot, G., Corrsin, S., 1971. Simple Eulerian time correlation of full- and narrow-band velocity signals in grid-generated, 'isotropic' turbulence. *J. Fluid Mech.*, 48, 273-337.

Favre, A.J., 1965. Review on Space-Time Correlations in Turbulent Fluids. *J. Appl. Mech.*, 32, 241-257.

Felder, S., Chanson, H., 2009. Turbulence, Dynamic Similarity and Scale Effects in High-Velocity Free-Surface Flows above a Stepped Chute. *Exp. Fluids*, 47, 1-18 (DOI: 10.1007/s00348-009-0628-3).

Felder, S., Chanson, H., 2012. Air-Water Flow Measurements in Instationary Free-Surface Flows: a Triple Decomposition Technique. Hydraulic Model Report No. CH85/12, School of Civil Engineering, The University of Queensland, Brisbane, Australia, 151 pages.

Fox J.F., Papaniclaou, A.N., Kjos, L., 2005. Eddy Taxonomy Methodology around Submerged Barb Obstacle within a Fixed Rough Bed. *Jl of Eng. Mech.*, ASCE, 131, 1082-1101.

Frisch, U., 1995. *Turbulence: The Legacy of A. N. Kolmogorov*. Cambridge University Press, 312 pages.

Harvey, A.C., 1993. *Time series models*. Harvester Wheatsheaf, London.

Herringe, R.A., Davis, M.R., 1976. Structural Development of Gas-Liquid Mixture Flows. *J. Fluid Mech.*, 73, 97-123.

Hussain, A.K.M.F., Reynolds, W.C., 1972. The Mechanics of an Organized Wave in Turbulent Shear Flow. Part 2: Experimental Results. *J. Fluid Mech.*, 54, 241-261.

Kipphan, H., 1977. Bestimmung von Transportkenngrößen bei Mehrphasenströmungen mit Hilfe der Korrelationsmeßtechnik. (Determination of Transport Parameters in Multiphase Flow with Aid of Correlation Measuring Technique.) *Chem.-Ing.-Techn.*, 49, 695-707 (in German).

Kökpınar, M.A., 2004. Flow over a Stepped Chute with and without Macro-Roughness Elements. *Can. Jl of Civil Eng.*, 31, 880-891.

Leandro, J., Carvalho, R., Chachereau, Y., Chanson, H., 2012. Estimating Void Fraction in a Hydraulic Jump by Measurements of Pixel Intensity. *Experiments in Fluids*, Vol. 52, No. 5, pp. 1307-1318 (DOI: 10.1007/s00348-011-1257-1).

Mossa, M., Tolve, U., 1998. Flow Visualization in Bubbly Two-Phase Hydraulic Jump. *Jl Fluids Eng.*, ASME, Vol. 120, March, pp. 160-165.

Press, H., Teukolsky, S.A., Vetterling, W.T., Flannery, B.P., 2007. *Numerical Recipes: The Art of Scientific Computing*. (3rd edition.) New York: Cambridge University Press.

Rao, N.S.L., Kobus, H.E., 1971. Characteristics of Self-Aerated Free-Surface Flows. *Water and Waste Water/Current Research and Practice*, 10. Eric Schmidt Verlag, Berlin, Germany.

Stern, R.M., Gouvea, E.B., Thattai, G., 2007. Polyaural array processing for automatic speech recognition in degraded environments. In *INTERSPEECH-2007*, 926-929.

Thorwarth, J., 2008. *Hydraulisches Verhalten der Treppengerinne mit eingetieften Stufen – Selbstinduzierte Abflussinstationaritäten und Energiedissipation*. (Hydraulics of Pooled Stepped Spillways – Self-induced Unsteady Flow and Energy Dissipation.) Ph.D. thesis, University of Aachen, Germany (in German).

Toombes, L., 2002. *Experimental Study of Air-Water Flow Properties on Low-Gradient Stepped Cascades*. Ph.D. thesis, Dept. of Civil Engineering, The University of Queensland, Australia.

Trahiotis, C., Bernstein, L.R., Stern, R.M., Buell T.N., 2005. Interaural correlation as a basis of a working model of binaural processing: An Introduction In A.N. Popper & R.R. Fay (Editors) "Sound Source Localization" New York: Springer, 238-271.

Wood, I.R., 1985. Air Water Flows. Proc. 21st IAHR Congress, Melbourne, Australia, Keynote address, pp. 18-29.

Wood, I.R., 1991. Air entrainment in free-surface flows. *IAHR Hydraulic Structures Design Manual No. 4, Hydraulic Design Considerations*, Balkema Publ., Rotterdam, The Netherlands, 149 pages.